An efficient kinetic modeling in plasmas by using the AWBS transport equation

Authors[a,1]

[a] *Centre Lasers Intenses et Applications, Universite de Bordeaux-CNRS-CEA, UMR 5107, F-33405 Talence, France*

Abstract

Keywords: kinetics; hydrodynamics; nonlocal electron transport; laser-heated plasmas.

*Corresponding author.
E-mail address: milan.holec@u-bordeaux.fr

1. Introduction

2. The AWBS nonlocal transport model

$$\frac{\partial f}{\partial t} + \boldsymbol{v}\cdot\nabla_{\boldsymbol{x}} f + \tilde{\boldsymbol{E}}\cdot\nabla_{\boldsymbol{v}} f = v\frac{\nu_e}{2}\frac{\partial}{\partial v}\left(f - f_M\right) + \frac{\nu_{ei} + \frac{\nu_e}{2}}{2}\frac{\partial^2 f}{\partial \boldsymbol{n}^2}, \tag{1}$$

[1]

3. BGK, AWBS, and Fokker-Planck models in local diffusive regime

We can try to find an approximate solution while using the first term of expansion in λ_e and muas

$$\tilde{f}(z,v,\mu) = f^0(z,v) + f^1(z,v)\lambda_{ei}(v)\mu. \tag{2}$$

3.1. The BGK local diffusive electron transport

$$\mu\left(\frac{\partial f}{\partial z} + \frac{\tilde{E}_z}{v}\frac{\partial f}{\partial v}\right) + \frac{\tilde{E}_z(1-\mu^2)}{v^2}\frac{\partial f}{\partial \mu} = \frac{f - f_M}{\lambda_e} + \frac{1}{2}\left(\frac{1}{\lambda_{ei}} + \frac{1}{2\lambda_e}\right)\frac{\partial}{\partial \mu}(1-\mu^2)\frac{\partial f}{\partial \mu}, \tag{3}$$

$$f^0 = f_M + \frac{1}{v}f^1\bar{Z}\lambda_{ei}^2, \tag{4}$$

$$f^1 = -\frac{\bar{Z}}{\bar{Z}+1}\left[\frac{\partial f^0}{\partial z} + \frac{\tilde{E}_z}{v}\frac{\partial f^0}{\partial v}\right], \tag{5}$$

$$f = f_M - \frac{\bar{Z}}{\bar{Z}+1}\left[\frac{1}{\rho}\frac{\partial \rho}{\partial z} + \left(\frac{v^2}{2v_{th}^2} - \frac{3}{2}\right)\frac{1}{T}\frac{\partial T}{\partial z} - \frac{\tilde{E}_z}{v_{th}^2}\right] f_M\lambda_{ei}\mu,$$

$$\boldsymbol{j} \equiv q_e\int_0^\infty\int_{4\pi} v\boldsymbol{n}f\,\mathrm{d}\boldsymbol{n}\ v^2\ \mathrm{d}v = \boldsymbol{0} \longrightarrow \tilde{\boldsymbol{E}} = v_{th}^2\left(\frac{\nabla\rho}{\rho} + \frac{5}{2}\frac{\nabla T}{T}\right), \tag{6}$$

$$f = f_M - \frac{\bar{Z}}{\bar{Z}+1}\left(\frac{v^2}{2v_{th}^2} - 4\right)\frac{1}{T}\frac{\partial T}{\partial z}f_M\lambda_{ei}\mu,$$

3.2. The AWBS diffusive electron transport

$$\mu\left(\frac{\partial f}{\partial z}+\frac{\tilde{E}_z}{v}\frac{\partial f}{\partial v}\right)+\frac{\tilde{E}_z(1-\mu^2)}{v^2}\frac{\partial f}{\partial \mu}=$$
$$\frac{v}{2\lambda_e}\frac{\partial}{\partial v}\left(f-f_M\right)+\frac{1}{2}\left(\frac{1}{\lambda_{ei}}+\frac{1}{2\lambda_e}\right)\frac{\partial}{\partial \mu}(1-\mu^2)\frac{\partial f}{\partial \mu}, \quad (7)$$

$$\begin{aligned}\frac{\partial}{\partial v}\left(f^0-f_M\right) &= \frac{1}{v^2}f^1\bar{Z}\lambda_{ei}^2, \qquad (8)\\ \frac{v}{\bar{Z}\lambda_{ei}}\frac{\partial(f^1\lambda_{ei})}{\partial v}-\frac{\bar{Z}+1}{\bar{Z}}f^1 &= \frac{\partial f^0}{\partial z}+\frac{\tilde{E}_z}{v}\frac{\partial f^0}{\partial v}\end{aligned}$$

$$\frac{\partial f^1}{\partial v}+\frac{1}{v}(3-\bar{Z})f^1=\frac{\bar{Z}}{v}\left(\frac{1}{\rho}\frac{\partial \rho}{\partial z}+\left(\frac{v^2}{2v_{th}^2}-\frac{3}{2}\right)\frac{1}{T}\frac{\partial T}{\partial z}-\frac{\tilde{E}_z}{v_{th}^2}\right)f_M. \quad (9)$$

3.3. The Fokker-Planck diffusive electron transport

$$v_{2th}=\sqrt{\frac{2k_BT}{m_e}}=1/j,$$

$$\begin{aligned}A &= -\frac{m_e^2v_{2th}^2\tilde{\boldsymbol{E}}}{2\pi e^4n_e\ln\Lambda}=-\frac{mE}{2\pi j^2e^3n_e\ln\Lambda},\\ B &= \frac{m_e^2v_{2th}^4|\nabla T|}{2\pi e^4n_e\ln\Lambda T}=\frac{2k_B^2T|\nabla T|}{\pi e^4n_e\ln\Lambda},\end{aligned}$$

$$\frac{A}{B}=-\frac{|\tilde{\boldsymbol{E}}|T}{v_{2th}^2|\nabla T|},$$

$$\tilde{\boldsymbol{E}}=-\frac{3}{2}\frac{v_{2th}^2}{2}\frac{\gamma_T}{\gamma_E}\frac{\nabla T}{T},$$

From Eq. (24) CSR, we can write the form of f_1 including both ∇T and $\tilde{\boldsymbol{E}}$ effects as

$$f_1(v,\theta)=\cos(\theta)\frac{B}{\bar{Z}}\left(d_T(v/v_{2th})+\frac{A}{B}d_E(v/v_{2th})\right)f_M(v),$$

	$\bar{Z}=1$	$\bar{Z}=2$	$\bar{Z}=4$	$\bar{Z}=16$	$\bar{Z}=116$
$\bar{\Delta}\boldsymbol{q}_{AWBS}$	0.057	0.004	0.038	0.049	0.004

Table 1: Relative error $\bar{\Delta}\boldsymbol{q}_{AWBS} = |\boldsymbol{q}_{AWBS} - \boldsymbol{q}_{SH}|/\boldsymbol{q}_{SH}$ of the AWBS kinetic model equation (1) showing the discrepancy (maximum around 5%) with respect to the original solution of the heat flux given by Spitzer and Harm [5].

where in the case of vanishing current one gets

$$\frac{A}{B} = \frac{3}{2}\frac{\gamma_T}{2\gamma_E},$$

i.e.

$$f_1(v,\theta) = \cos(\theta)\frac{m_e^2}{4\pi e^4 \ln\Lambda}\frac{v_{2th}^4}{\bar{Z}}\left(2d_T(v/v_{2th}) + \frac{3}{2}\frac{\gamma_T}{\gamma_E}d_E(v/v_{2th})\right)\frac{f_M(v)}{n_e}\frac{\nabla T}{T}, \tag{10}$$

where $d_T(x) = \bar{Z}D_T(x)/B$ and $d_E(x) = \bar{Z}D_E(x)/A$ are represented by numerical values in TABLE I and TABLE II in [5], respectively. In the case of high $\bar{Z}$ limit, $\gamma_T \to 1$, $\gamma_E \to 1$, $d_E(x) = x^4$, and $d_T(x) = x^4(2.5 - x^2)/2$ [5], which leads to the standard Lorentz gas model

$$f_1(v,\theta) = \cos(\theta)\frac{m_e^2}{4\pi e^4 \ln\Lambda}\frac{v^4}{\bar{Z}}\left(4 - \frac{v^2}{v_{2th}^2}\right)\frac{f_M(v)}{n_e}\frac{\nabla T}{T}, \tag{11}$$

[2], [3], [4]

3.4. Summary of BGK, AWBS, and Fokker-Planck diffusion

4. Benchmarking the AWBS nonlocal transport model

4.1. Review of simulation codes

4.2. C7

In order to eliminate the dimensions of the above transport problem the first-two-moment model based on approximation

$$f = \frac{f_0}{4\pi} + \frac{3}{4\pi}\boldsymbol{n}\cdot\boldsymbol{f_1},$$

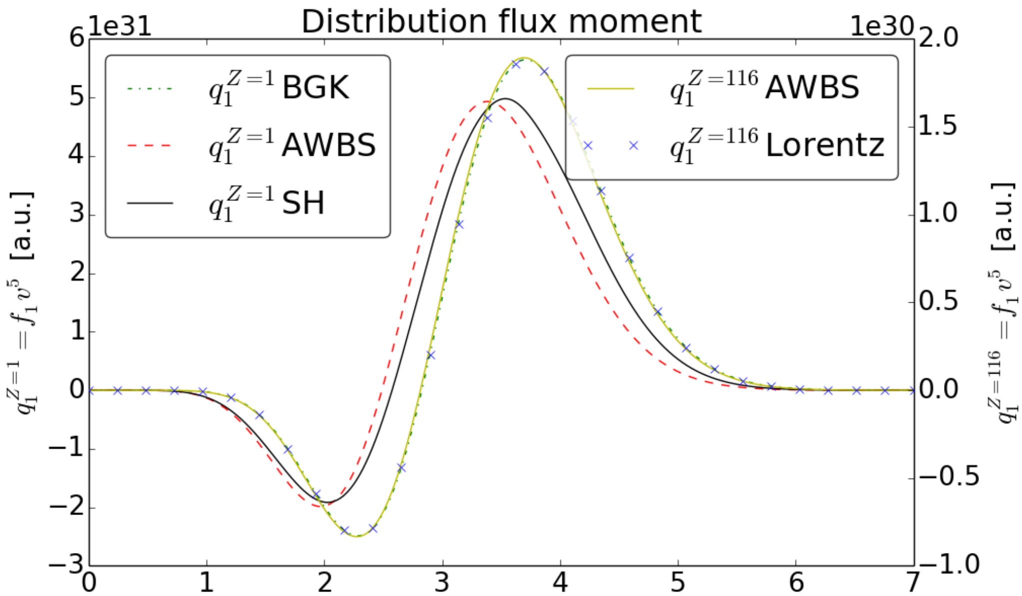

Figure 1: The flux velocity moment of the anisotropic part of the electron distribution function in low $Z = 1$ and high $Z = 116$ plasmas in diffusive regime.

can be adopted and reads

$$\begin{aligned} v\frac{\nu_e}{2}\frac{\partial}{\partial v}\left(f_0 - 4\pi f_M\right) &= v\nabla\cdot\boldsymbol{f_1} + \tilde{\boldsymbol{E}}\cdot\frac{\partial \boldsymbol{f_1}}{\partial v} + \frac{2}{v}\tilde{\boldsymbol{E}}\cdot\boldsymbol{f_1}, \\ v\frac{\nu_e}{2}\frac{\partial \boldsymbol{f_1}}{\partial v} - \left(\nu_{ei} + \frac{\nu_e}{2}\right)\boldsymbol{f_1} &= \frac{v}{3}\nabla f_0 + \frac{\tilde{\boldsymbol{E}}}{3}\frac{\partial f_0}{\partial v}, \end{aligned}$$

$$\boldsymbol{q}_c \equiv q_e \int_v \left(\frac{\nu_e v^2}{\nu_{ei} + \frac{\nu_e}{2}}\frac{\partial \boldsymbol{f_1}}{\partial v} - \frac{v^2}{3\left(\nu_{ei} + \frac{\nu_e}{2}\right)}\nabla f_0 - \frac{v}{3\left(\nu_{ei} + \frac{\nu_e}{2}\right)}\frac{\partial f_0}{\partial v}\tilde{\boldsymbol{E}}\right) v^2\,\mathrm{d}v = 0,$$

4.2.1. Nonlocal electric field treatment

$$\begin{aligned} &\left(v\frac{\nu_e}{2} - \frac{2\tilde{E}_z^2}{3v\nu_e}\right)\frac{\partial f_{1_z}}{\partial v} = \\ &\qquad \frac{2\tilde{E}_z}{3\nu_e}\frac{\partial f_{1_z}}{\partial z} + \frac{4\pi\tilde{E}_z}{3}\frac{\partial f_M}{\partial v} + \frac{v}{3}\frac{\partial f_0}{\partial z} + \left(\frac{4\tilde{E}_z^2}{3v^2\nu_e} + \left(\nu_{ei} + \frac{\nu_e}{2}\right)\right) f_{1_z}, \end{aligned}$$

Kn	10^{-3}	5×10^{-3}	10^{-2}	5×10^{-2}	10^{-1}
$v_{lim}^{Z=2}/v_{th}$	14.8	6.8	5.0	2.8	2.6
$v_{lim}^{Z=10}/v_{th}$	6.7	3.4	2.6	1.6	1.3

Table 2: $\sqrt{3}v\frac{\nu_e}{2} > \tilde{E}_z$.

$$|\tilde{\boldsymbol{E}}_{red}| = v\nu_e + \alpha^E v\nu_e, \tag{12}$$

$$\begin{aligned} |\tilde{\boldsymbol{E}}_{red}| &= |\tilde{\boldsymbol{E}}_d| + |\tilde{\boldsymbol{E}}_{iso}|, \\ v\nu_e + |\tilde{\boldsymbol{E}}_{iso}| &= |\tilde{\boldsymbol{E}}_d|, \end{aligned}$$

where we define the isotropic effect of E field as $|\boldsymbol{E}_{iso}| = v\nu_e^E$ by introducing the effective collisional frequency ν_e^E.

Since the effect of the original E field $\tilde{\boldsymbol{E}}$ has been reduced in (12), an additional collision term

$$v\nu_{ei}^E = |\tilde{\boldsymbol{E}}| - |\tilde{\boldsymbol{E}}_{red}|,$$

is added to scattering on ions. The improved collision AWBS operator then takes the following form

$$C_{AWBS} = v\left(\frac{1}{2} + \alpha^E\right)\nu_e\frac{\partial}{\partial v}\left(f - f_M\right) + \left(\nu_{ei} + \nu_{ei}^E + \frac{\nu_e}{2}\right)\left(f_0 - f\right),$$

where both α^E and ν_{ei}^E apply only if $|\tilde{\boldsymbol{E}}| > \sqrt{3}v\frac{\nu_e}{2}$ and are set to zero otherwise.

P1 approximation equivalent

$$f = \frac{4\pi f_M + \delta f_0}{4\pi} + \frac{3}{4\pi}\boldsymbol{n}\cdot\boldsymbol{f_1}. \tag{13}$$

where the moment model reads

$$
\begin{aligned}
v\left(\frac{1}{2}+\alpha^E\right)\nu_e\frac{\partial \delta f_0}{\partial v} &= v\nabla\cdot\boldsymbol{f_1}+\tilde{\boldsymbol{E}}\cdot\left(\omega_d\frac{\partial \boldsymbol{f_1}}{\partial v}+\frac{2}{v}\boldsymbol{f_1}\right),\\
v\left(\frac{1}{2}+\alpha^E\right)\nu_e\frac{\partial \boldsymbol{f_1}}{\partial v} &= \left(\nu_{ei}+\nu_{ei}^E+\frac{\nu_e}{2}\right)\boldsymbol{f_1}+\frac{v}{3}\nabla\left(4\pi f_M+\delta f_0\right)\\
&\quad+\frac{\tilde{\boldsymbol{E}}}{3}\left(4\pi\frac{\partial f_M}{\partial v}+\omega_d\frac{\partial \delta f_0}{\partial v}\right),
\end{aligned}
$$

$$
\tilde{\boldsymbol{E}}=\frac{\int_v\left(\frac{\left(\frac{1}{2}+\alpha^E\right)\nu_e v^2}{\nu_{ei}+\nu_{ei}^E+\frac{\nu_e}{2}}\frac{\partial \boldsymbol{f_1}}{\partial v}-\frac{v^2}{3\left(\nu_{ei}+\nu_{ei}^E+\frac{\nu_e}{2}\right)}\nabla\left(4\pi f_M+\delta f_0\right)\right)v^2\,\mathrm{d}v}{\int_v\frac{v}{3\left(\nu_{ei}+\nu_{ei}^E+\frac{\nu_e}{2}\right)}\left(4\pi\frac{\partial f_M}{\partial v}+\omega_d\frac{\partial \delta f_0}{\partial v}\right)v^2\,\mathrm{d}v},
$$

where $\omega_d(v)=|\tilde{\boldsymbol{E}}_d(v)|/|\tilde{\boldsymbol{E}}|$.

4.3. Aladin

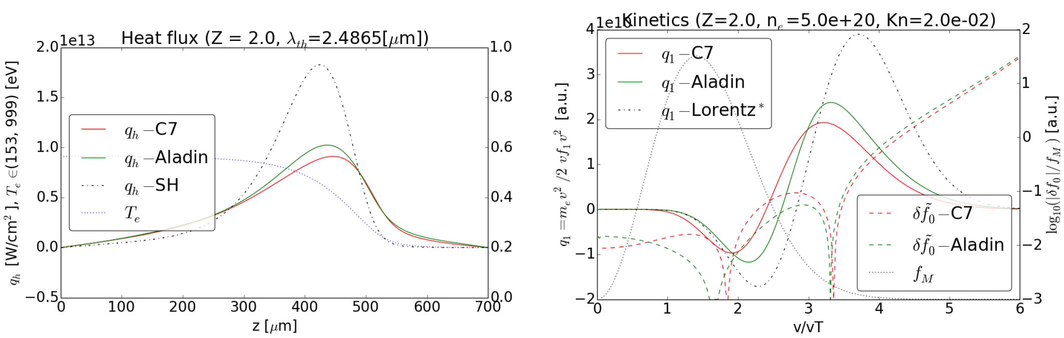

Figure 2: Snapshot 12 ps. Left: correct steady solution of heat flux. Right: correct comparison to kinetic profiles at point 442 μm by Aladin.

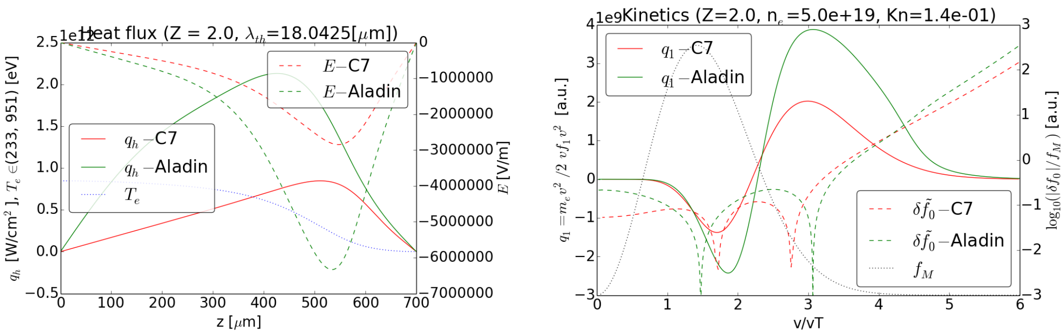

Figure 3: Snapshot 12 ps. Left: correct steady solution of heat flux. Right: correct comparison to kinetic profiles at point 480 μm by Aladin.

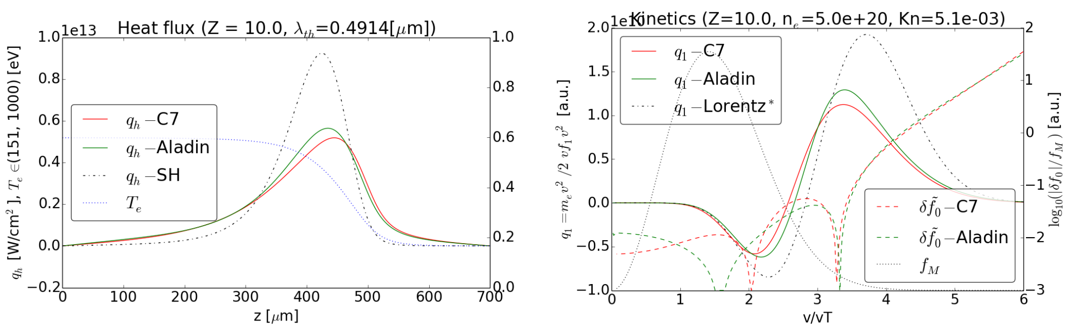

Figure 4: Snapshot 12 ps. Left: correct steady solution of heat flux. Right: correct comparison to kinetic profiles at point 442 μm by Aladin.

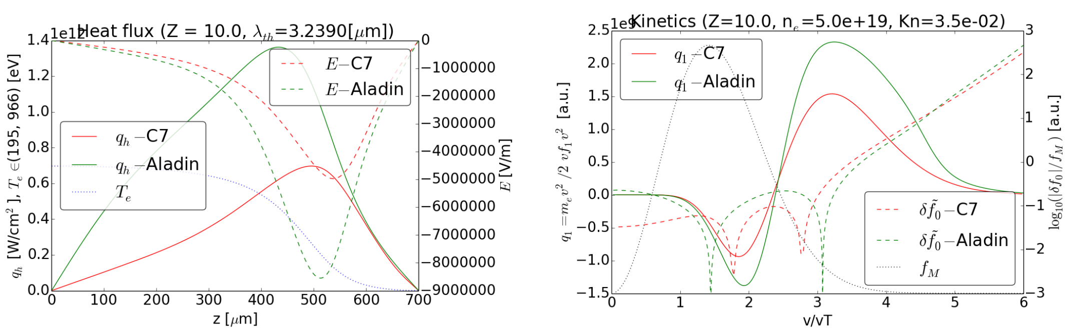

Figure 5: Snapshot 12 ps. Left: correct steady solution of heat flux. Right: correct comparison to kinetic profiles at point 480 μm by Aladin.

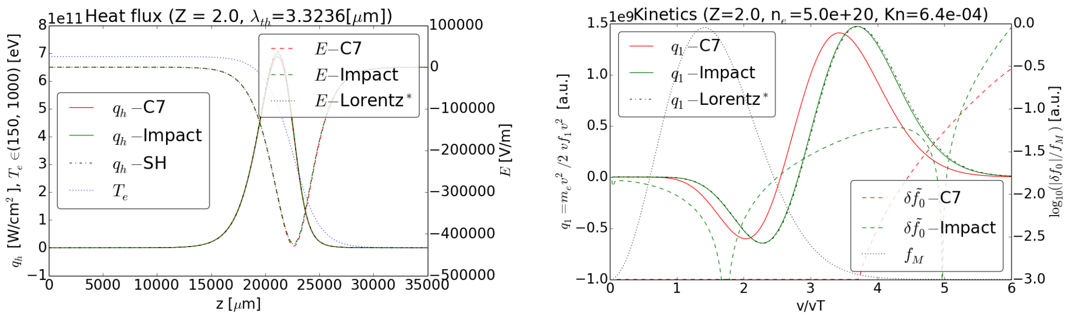

Figure 6: Impact diffusive case 1.

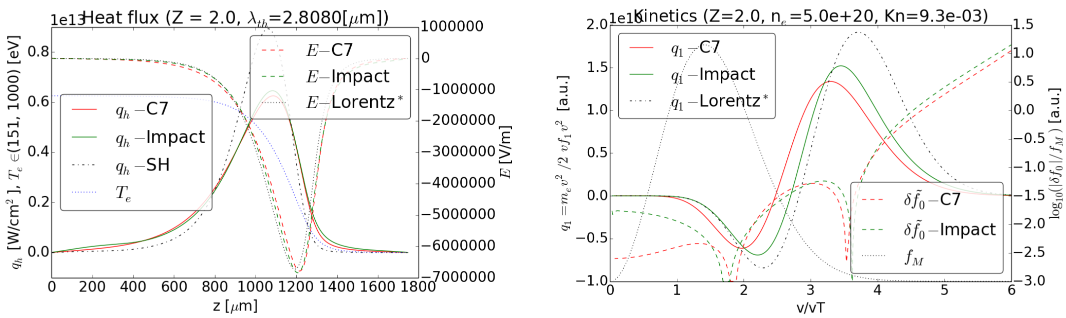

Figure 7: Impact case 2.

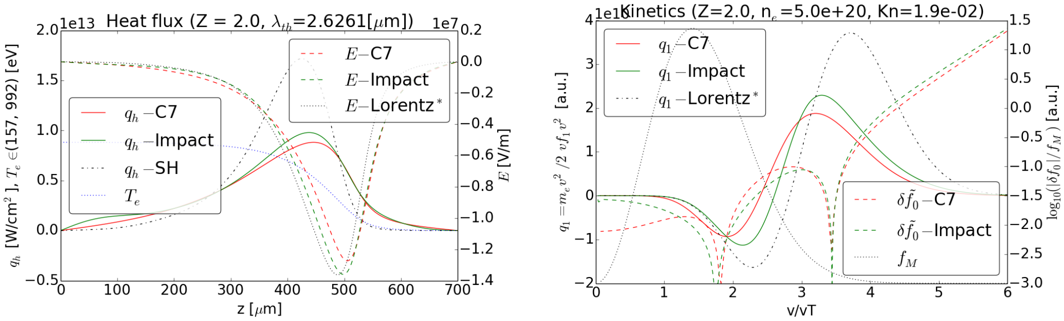

Figure 8: Snapshot 12 ps. Left: correct steady solution of heat flux. Right: correct comparison to kinetic profiles at point 437 μm by Impact.

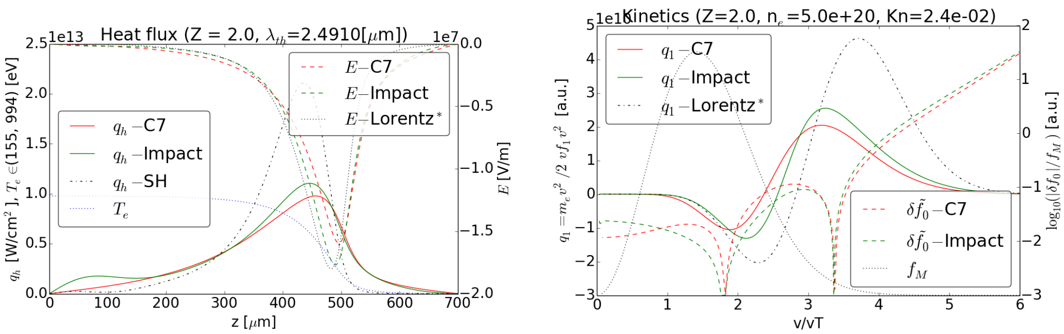

Figure 9: Impact case 4.

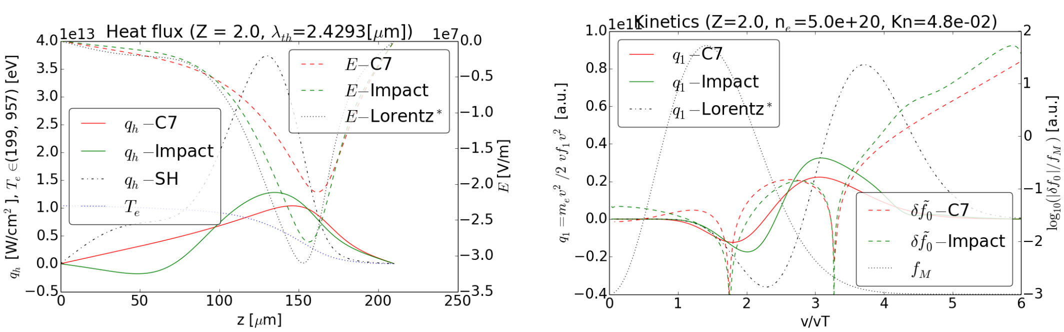

Figure 10: Impact case 5.

4.5. Calder

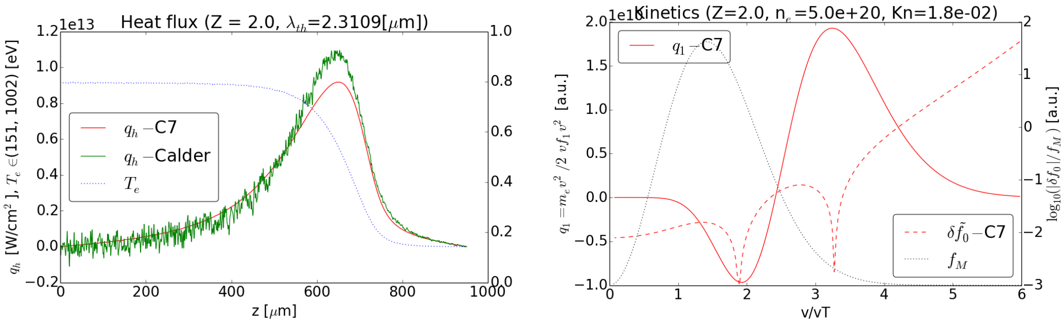

Figure 11: Snapshot 11 ps. Left: correct steady solution of heat flux. Right: Kinetic profiles at point of maximum flux by C7. Kinetics profiles by CALDER should be added.

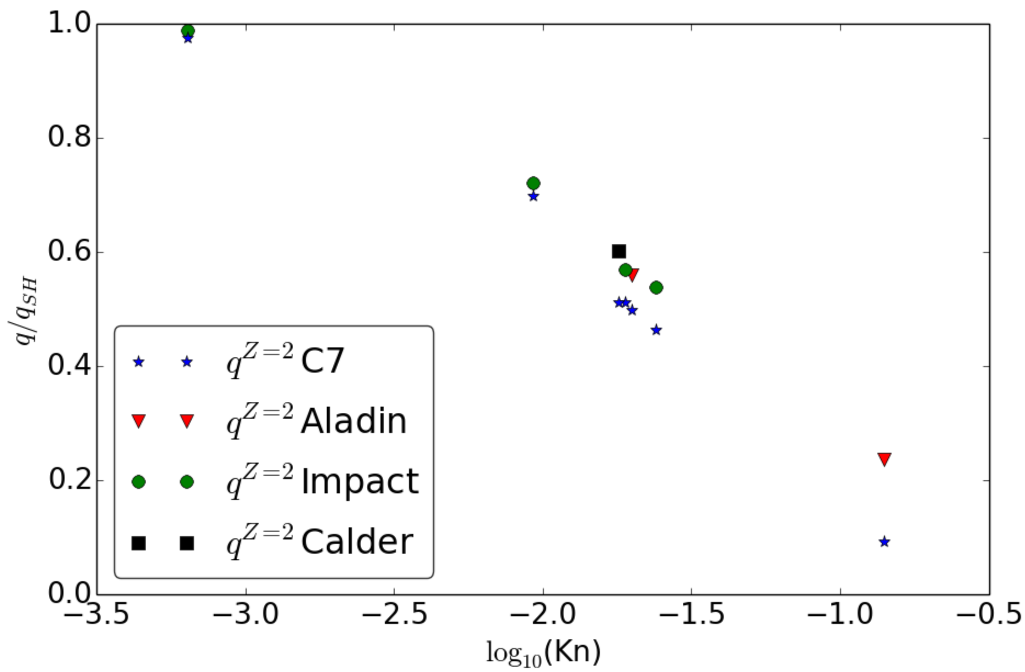

Figure 12: Simulation results for the case $Z = 2$ computed by C7/Aladin/Impact/Calder. Every point corresponds to the maximum heat flux in a "tanh" temperature simulation, which can be characterized by Kn. The range of $\log_{10}(\text{Kn}) \in (-0.5, -3.5)$ can be expressed as equivalent to the electron density approximate range $\text{n}_e \in (5e19, 3.5e22)$ of the 50 μm slope tanh case.

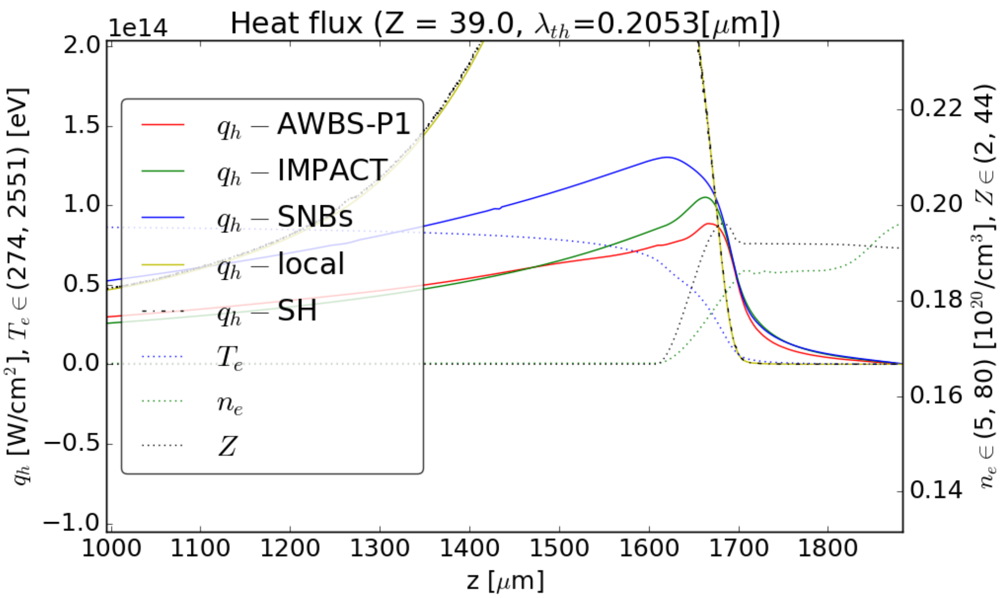

Heat flux (Z = 39.0, λ_{th}=0.2053[μm])
1e14
q_h [W/cm^2], $T_e \in$ (274, 2551) [eV]
$n_e \in$ (5, 80) [10^{20}/cm^3], $Z \in$ (2, 44)
z [μm]
$q_h -$ AWBS-P1
$q_h -$ IMPACT
$q_h -$ SNBs
$q_h -$ local
$q_h -$ SH
T_e
n_e
Z

Figure 13:

5. Conclusions

[1] Nathaniel J. Fisch. Theory of current drive in plasmas. Rev. Mod. Phys., 59(1):175234, Jan 1987.

[2] Marshall N. Rosenbluth, William M. MacDonald, and David L. Judd. Fokker-planck equation for an inverse-square force. Phys. Rev., 107(1):16, Jul 1957.

[3] Longmire, Conrad L. : Elementary Plasma Physics. Intersci. Pub., 1963.

[4] I.P. Shkarofsky, T.W. Johnston, T.W. Bachynski, The Particle Kinetics of Plasmas, Addison-Wesley, Reading, MA, 1966.

[5] SH 1953.